Anionic organo-hydrogel electrolyte with enhanced ionic conductivity and balanced mechanical properties for flexible supercapacitors

Ye Yang[1], Kun-Peng Wang[1], Qian Zang, Qiqi Shi, Yiwei Wang, Zhenyu Xiao, Qi Zhang*, and Lei Wang*

State Key Laboratory Base of Eco-Chemical Engineering, Taishan Scholar Advantage and Characteristic Discipline Team of Eco Chemical Process and Technology, College of Chemistry and Molecular Engineering, Qingdao University of Science and Technology, Qingdao 266042, China.

[1] These authors contributed equally to this work.

E-mail: zhangqi@qust.edu.cn (Qi Zhang), inorchemwl@126.com (Lei Wang).

1. Experimental

Materials: Poly(vinyl alcohol) (PVA, n=approx. 1700 degree of saponification 97.0 to 100.0 mol % TCI), KOH (AR Sinopharm Chemical Reagent), carboxymethyl cellulose sodium (CMC, 800 ~ 1200Pa·s Sinopharm Chemical Reagent), Activated carbon (AC, XFNANO), polytetrafluoroethylene (PTFE, D210C DAIKIN). λ-Carrageenan (LC, Aladdin). ethylene glycol (EG, Sinopharm Chemical Reagent).

Preparation of the hydrogel electrolyte: Typically, certain quality of CMC was dissolving into the mixed solvent EG/H_2O (v/v=2:1) to get CMC solution. Then, 0.75 g PVA and 0.15 g LC were added to the above solution in sequence with continuous stirring at room temperature for 1 h and heated to 90 ^{o}C to get a clear viscous solution. Pouring the solution into the PTFE mold and freeze it at -20 ^{o}C for 24 h to get the original PVA-CMC-LC organo-hydrogel. By varying the CMC contents, three different PVA-CMC$_x$-LC$_y$ organo-hydrogels were obtained (x refers to the weight of CMC: 0.1, 0.15, 0.2). After thawing it at room temperature for 4 h, the products were soaked into

6 M KOH solution for 12 h to balance charge and generate ionic conductive organo-hydrogels. For comparison, the corresponding hydrogels are prepared with the similar processdure without the addition of EG.

Assemble of symmetric SCs device: The symmetric SCs device was assembled with AC as the electrode material and the organo-hydrogel and hydrogel as the electrolyte. The active carbon electrode was prepared by mixing the PTFE aqueous solution (10wt%), the acetylene black (10wt%) and the activated carbon (80wt%) in the NMP and ultrasound for 30 min to form a homogeneous suspension. The suspension was dried in a 120°C vacuum oven for 12 h to remove the solvent. Finally, the dried slurry was pressed on NF to obtain an AC electrode. Then sandwich the prepared gel electrolyte between the two AC electrodes to get the symmetric SC device.

Material characterization: The morphology of PVA-CMC-LC organo-hydrogel was analyzed by Scanning Electronic Microscope (JEOL, JSM-7900F). The tensile and compressive properties of the gels were tested on a universal tensile testing machine (Zwick Roell, Z005). Tensile tests are conducted on a rectangular shape at 20 mm min^{-1}, and the compressive tests are carried out on cylindrical shapes with 1 cm in diameter and 3 cm in height at the compressive rate of 5 mm min^{-1}. The characterization of functional groups of the gels tested by fourier transform infrared spectroscopy (FT-IR, Thermo Scientific Nicolet IS10). The thermogravimetric analysis (TGA) curves were performed using a thermal analyzer (NETZSCH, STA 449 F5).

Characterizations of the organo-hydrogel electrolyte: All the electrochemical tests including cyclic voltammetry (CV), galvanostatic charging-discharging (GCD), electrochemical impedance spectroscopy (EIS), and ionic conductivity (σ) were carried out in the two-electrode system on CHI760E (Shanghai, China) and LANDIAN (Wuhan, China). Then the specific capacitance (C and Cs, F g^{-1}), energy density (E, Wh kg^{-1}) and power density (P, W kg^{-1}) were calculated by the following equations:

$$C=(I\times\Delta t)/\Delta V \qquad (1)$$

$$Cs=4\times C \qquad (2)$$

$$E=(C\times\Delta V^2)/7.2 \qquad (3)$$

$$P=(3600\times E)/\Delta t \qquad (4)$$

The ionic conductivity (σ, S m^{-1}) of the organo-hydrogels was calculated by the following equation, where L, A represent the thickness and the contact area of the gel, R is the impendence value from EIS. In this work, the thickness is 0.2 cm and the contact area is 2 cm^{-2}.

$\sigma=(d\times100)/(A\times R)$ (5)

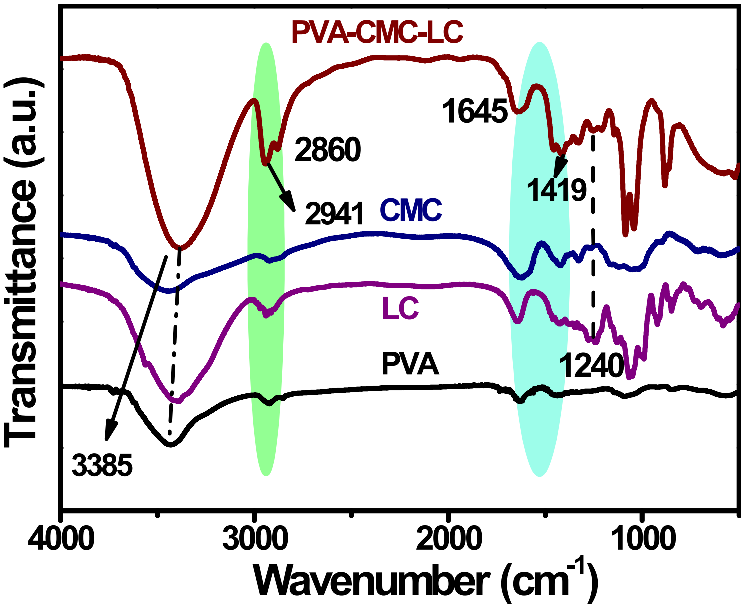

Figure S1. FT-IR spectra of the PVA, LC, CMC, and PVA-CMC-LC.

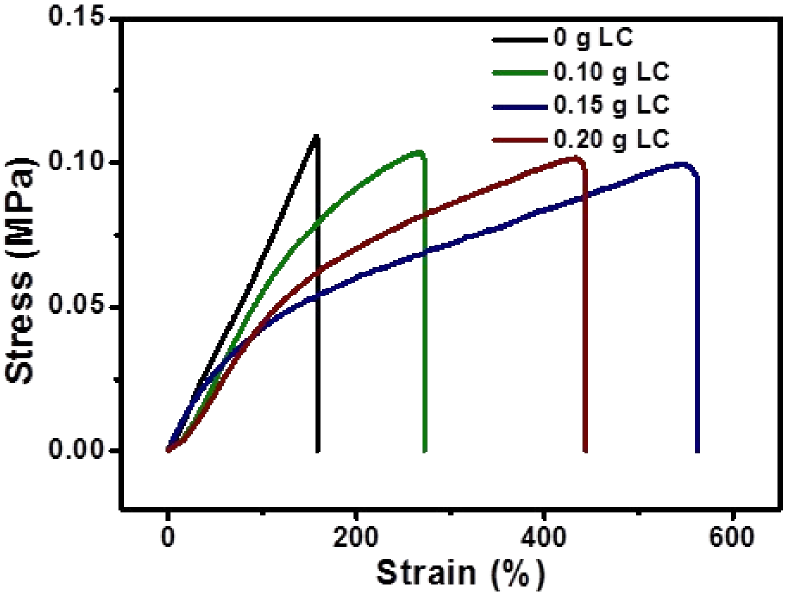

Figure S2. Tensile stress-strain curves of PVA-$CMC_{0.15}$-LC_y (y changes from 0 to 0.2) organo-hydrogels.

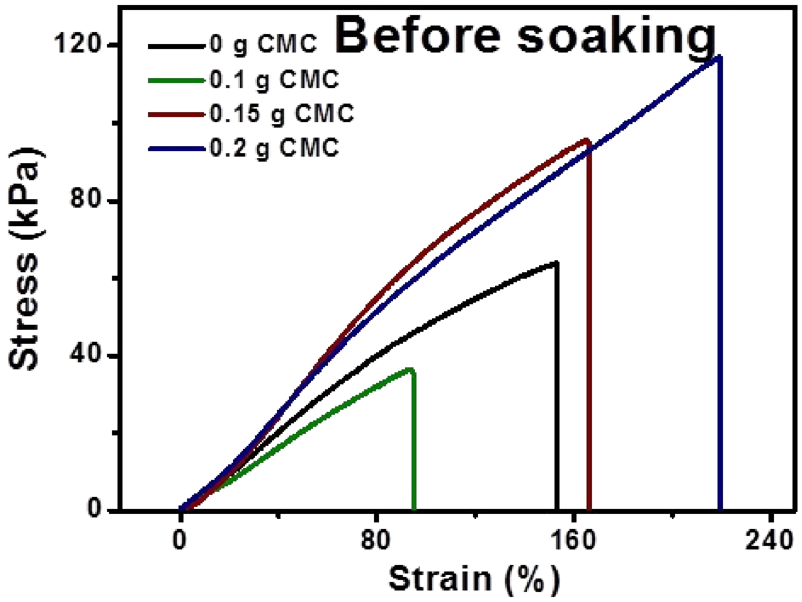

Figure S3. Tensile stress-strain curve of PVA-CMC$_x$-LC$_{0.15}$ (x changes from 0 to 0.2) organo-hydrogel before soaking KOH .

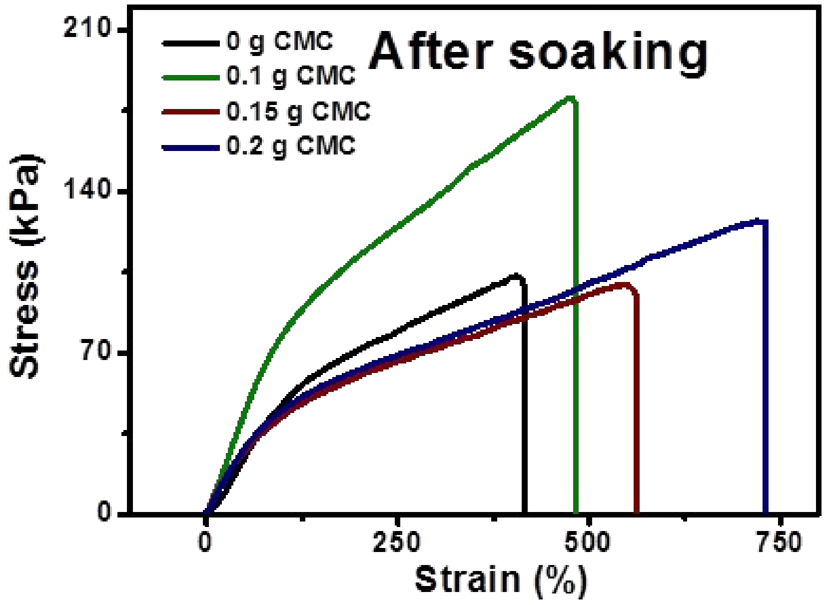

Figure S4. Tensile stress-strain curve of PVA-CMC$_x$-LC$_{0.15}$ (x changes from 0 to 0.2) organo-hydrogel after soaking KOH.

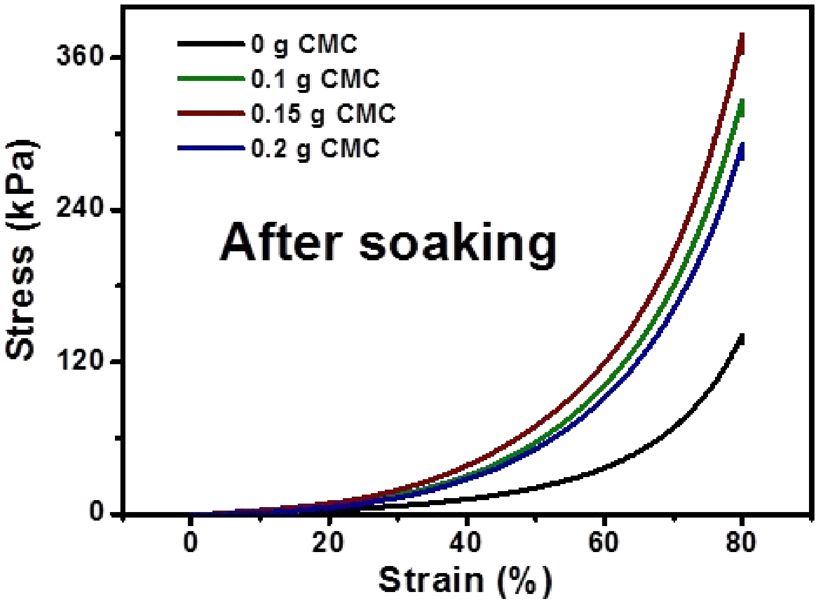

Figure S5. Compressive stress-strain curve of PVA-CMC$_x$-LC$_{0.15}$ (x changes from 0 to 0.2) organo-hydrogel after soaking KOH.

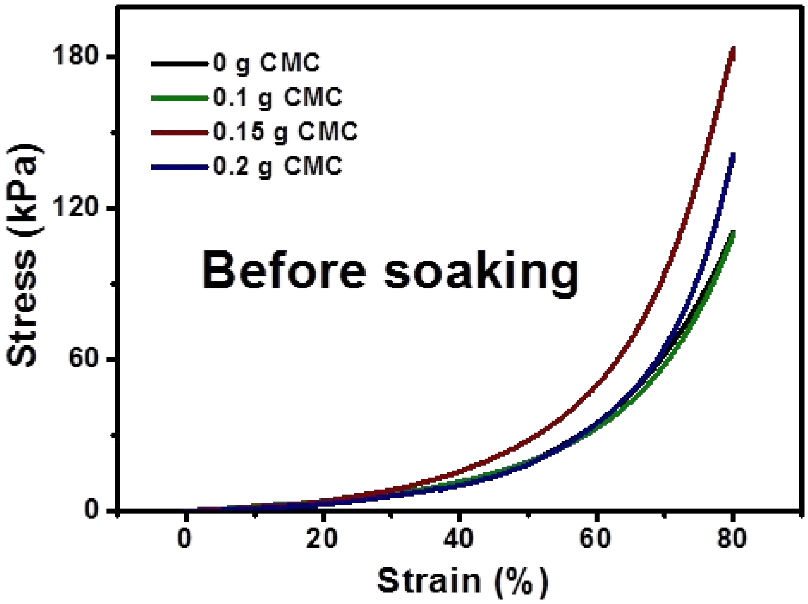

Figure S6. Compressive stress-strain curve of PVA-CMC$_x$-LC$_{0.15}$ (x changes from 0 to 0.2) organo-hydrogel before soaking KOH.

Table S1. The comparison in mechanical performance of PVA-CMC-LC organo-hydrogel and other previous reports.

Electrolytes	**Stretch**		**Compression**		**Ref**
	Strain (%)	**Stress** (MPa)	**Strain (%)**	**Stress** (MPa)	
PVA-CMC-LC	562	0.1	80	0.4	This work
PVA/CH_3COONa/ glycerol	200	0.29			1
KCl-Fe^{3+}/PAA	700	0.4			4
PZHE	500	0.1	75	0.7	17
AF PVA-CMC/$Zn(CF_3SO_3)_2$	423.1	0.51	75	0.2	18
PAM-co-PAA/k-CG/$ZnSO_4$	626	0.042	60	0.15	19
PAM/SA	2400	0.5	90	0.95	20
poly($HFBA_8$-co-$HEMA_1$)	305	0.028			21
CG/PAAm-7Li/K	567.7	0.24			22
PMEL	1050	0.07			23
PVA/PAS-ILs	300	1.9			24

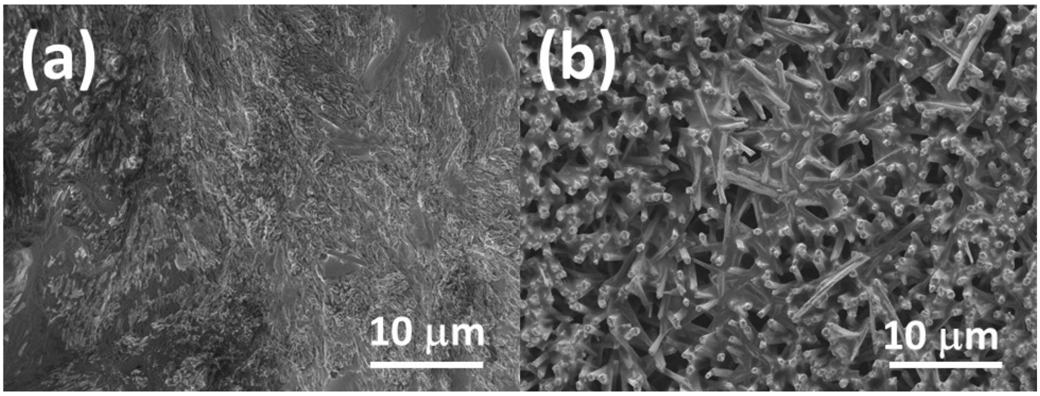

Figure S7. SEM images of PVA-CMC-LC organo-hydrogel before and after immersing in KOH solution

DFT calculations

Calculations were performed under B3LYP density functional and 6-31G(d) basis set with empirical correlation (using keyword "em=GD3BJ") in Gaussian 09. All the structures were optimized and certified without imaginary frequencies. In demand of considering basis set superposition error (BSSE, using key word "counterpoise=2") towards complex interaction. The corrected complexation energy was detailed in Table S2 and S3.

Table S2. Calculation of interaction energy of various components with EG molecules.

Model	E_{int} (kcal mol^{-1})	E(A···B)*	E(A)+E(B)*	BSSE*
PVA-EG	-7.58	-732.2711	-732.2590	0.0105
CMC-EG	-40.31	-1599.1400	-1599.0758	0.0174
LC-EG	-28.01	-3397.8428	-3397.7982	0.0093

*Energy values given as Hartree.

Table S3. Calculation of interaction energy of various components with water molecules

Model	E_{int} (kcal mol^{-1})	E(A···B)*	E(A)+E(B)*	BSSE*
H_2O-H_2O	-3.54	-152.8232	-152.8175	0.0029
EG-H_2O	-5.02	-306.6527	-306.6447	0.0057
PVA-H_2O	-4.27	-578.4350	-578.4282	0.0070
CMC-H_2O	-25.62	-1445.2952	-1445.2544	0.0118
LC-H_2O	-12.99	-3243.9787	-3243.9580	0.0063

*Energy values given as Hartree.

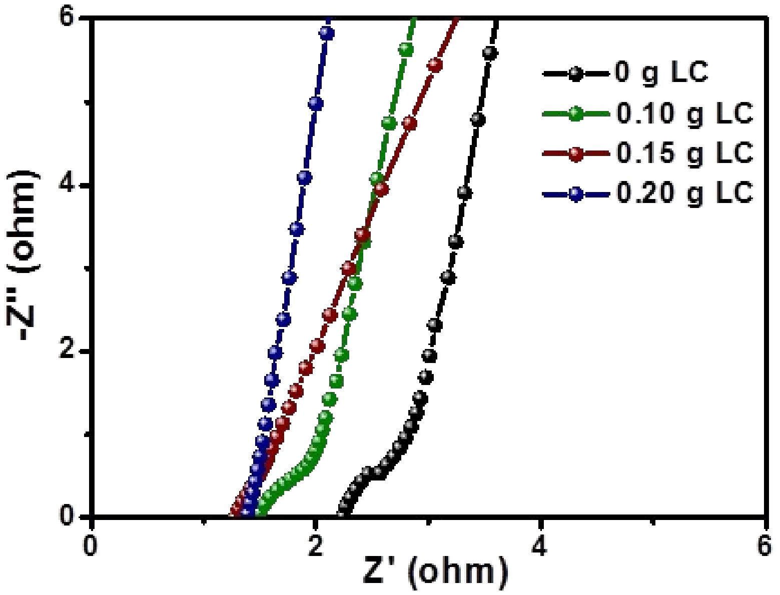

Figure S8. The Nyquist plots of PVA-$CMC_{0.15}$-LC_y (y changes from 0 to 0.2) organo-hydrogel.

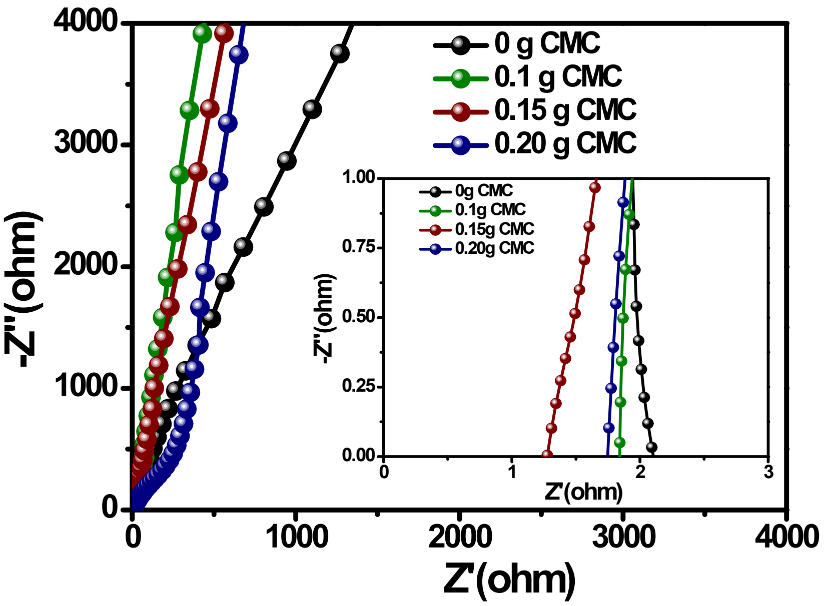

Figure S9. The Nyquist plots of PVA-CMC$_x$-LC$_{0.15}$ (x changes from 0 to 0.2) organo-hydrogel.

Table S4. The comparison in ionic conductivity of PVA-CMC-LC organo-hydrogel and other previous reports.

Electrolytes	Ionic conductivity (S m^{-1})	References
PVA-CMC-LC	8.3	This work
PVA/CH_3COONa/glycerol	8.127	1
PVA/Agar-EMIMBF$_4$-Li_2SO_4	4.36	2
AG/PAAm/LiCl	1.3±0.8	3
KCl–Fe^{3+}/PAA	0.09	4
HA-GPE	3.11	5
SPI-PAAm	1.634	6
Al-alginate/PAAm	3	7
PAD/H_2SO_4	5.7	8
OHEC	2.29	9

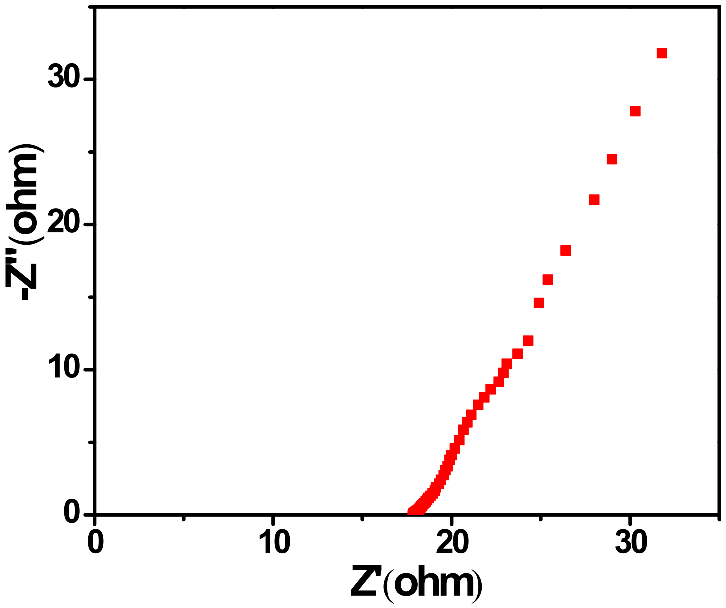

Figure S10. The Nyquist plots of the PVA-CMC-LC organo-hydrogel immersing in KOH solution with EG and H_2O mixed solvent.

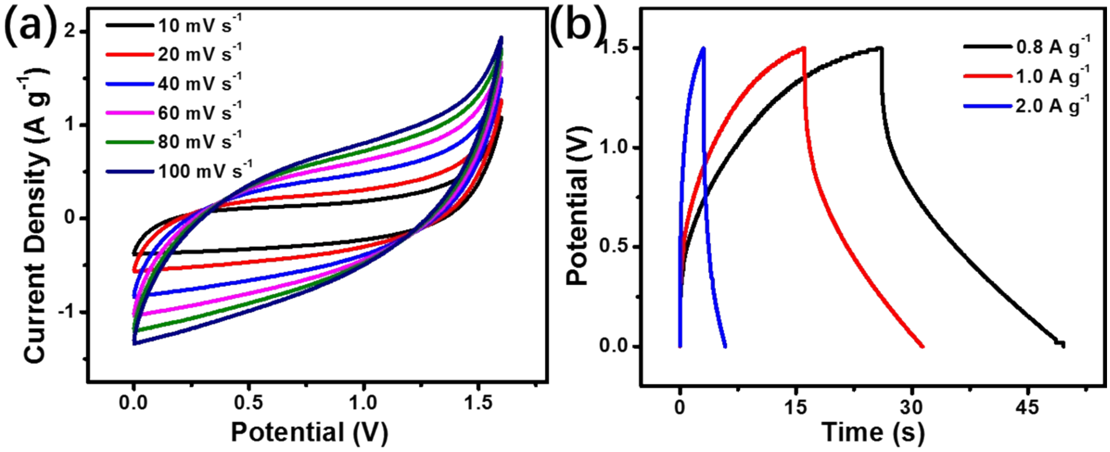

Figure S11. The CV and GCD curves of the SCs devices based on PVA-CMC-LC organo-hydrogel immersing in KOH solution with EG and H_2O mixed solvent.

Table S5. Quality change of the PVA-CMC$_x$-LC$_{0.15}$ organo-hydrogel with different CMC contents before and after soaking in 6 M KOH

CMC content (g)	Original weight (g)	Weight after soaking (g)	Percentage
0	0.3826	0.293	76.6%
0.10	0.3732	0.3798	101.8%
0.15	0.3029	0.3719	122.8%
0.20	0.3033	0.3607	118.9%

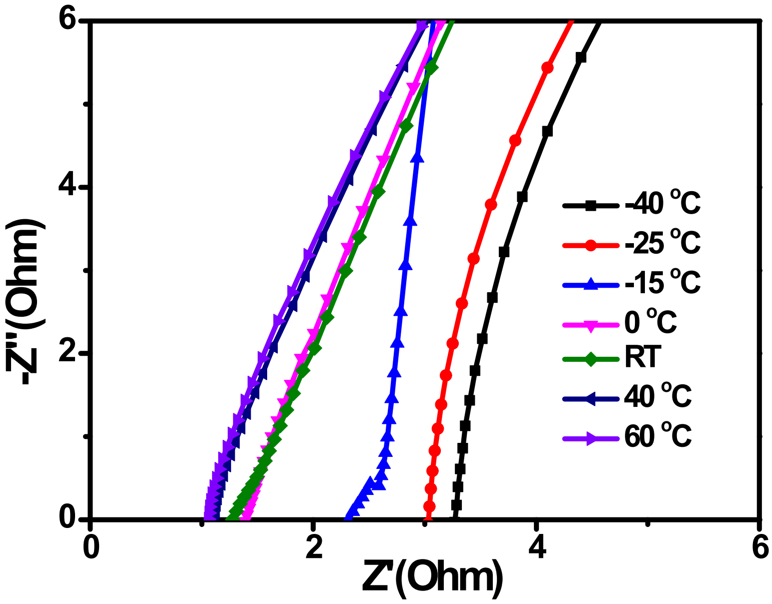

Figure S12. The Nyquist plots of PVA-CMC-LC organo-hydrogel at a wide temperature range from -40 to 60 °C.

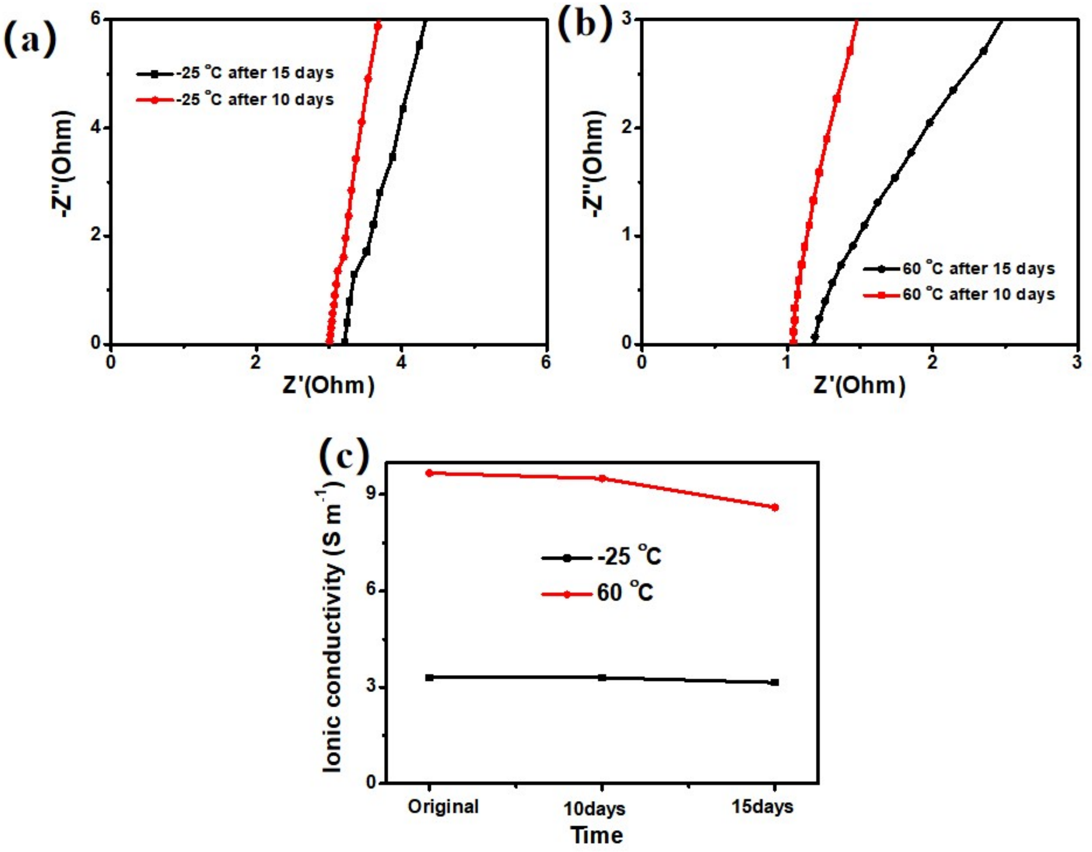

Figure S13. The stability of the organo-hydrogel at -25 and 60 °C. (a,b) the Nyquist plots and (c)the change in ionic conductivities.

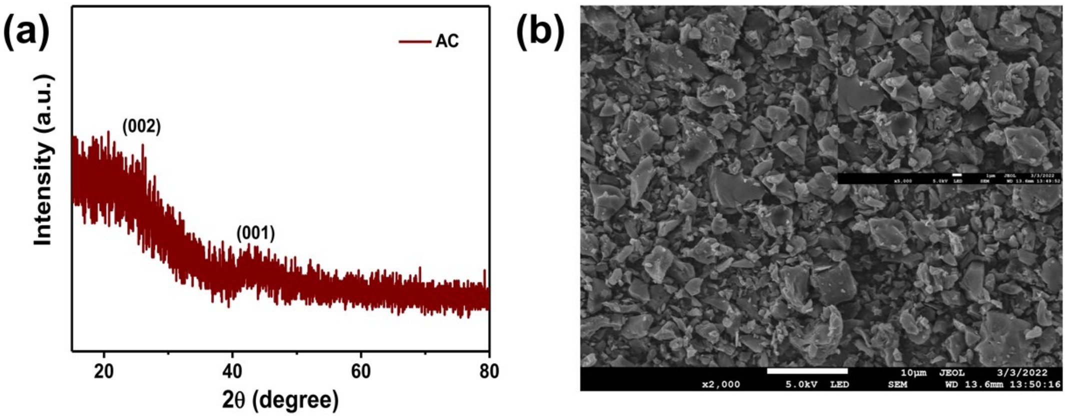

Figure S14. The XRD and SEM of AC (active carbon).

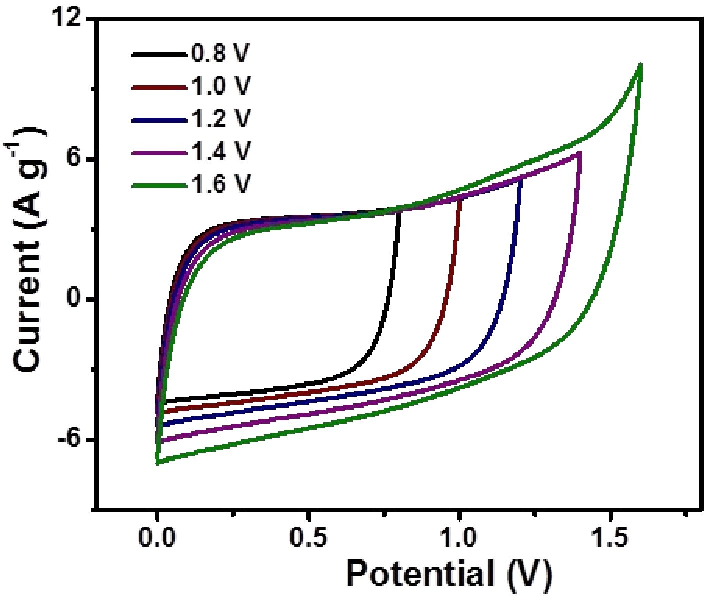

Figure S15. The CV curves of the SCs devices based on PVA-CMC-LC organo-hydrogel with different cut-off potential range from 0.8-1.6 V at room temperature.

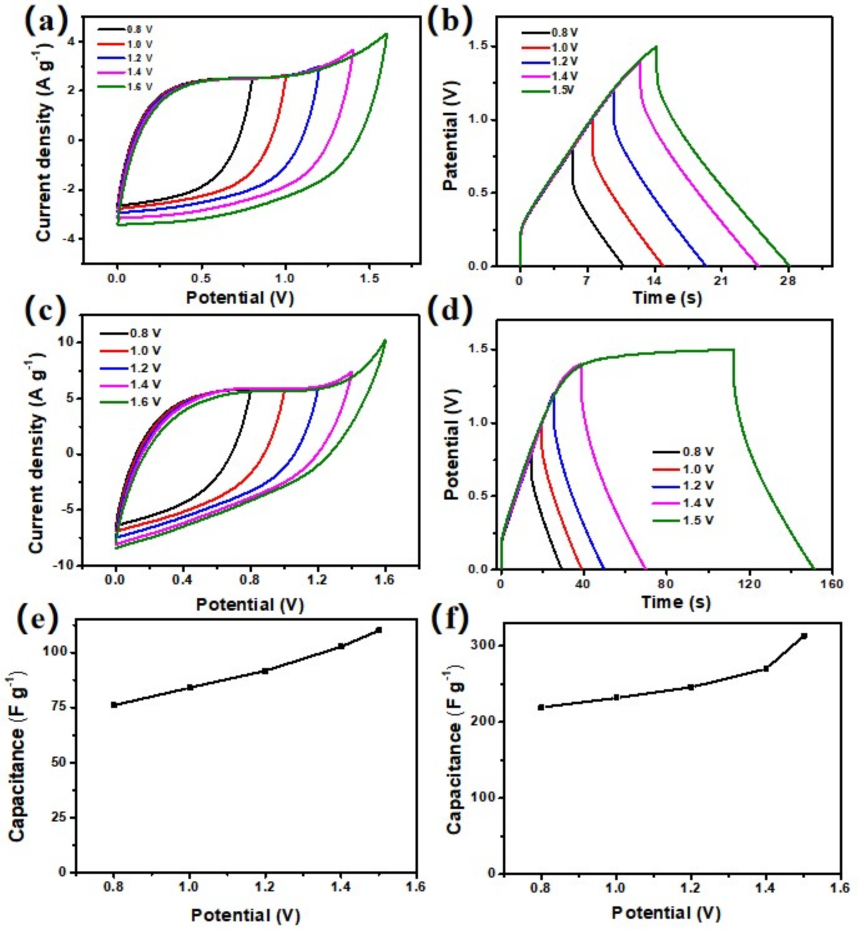

Figure S16. The CV, GCD, and capacitance curves of the SCs devices based on PVA-CMC-LC organo-hydrogel with different cut-off potential range at -40 ^{o}C (a,b,e) and

60 °C (c,d,f), respectively.

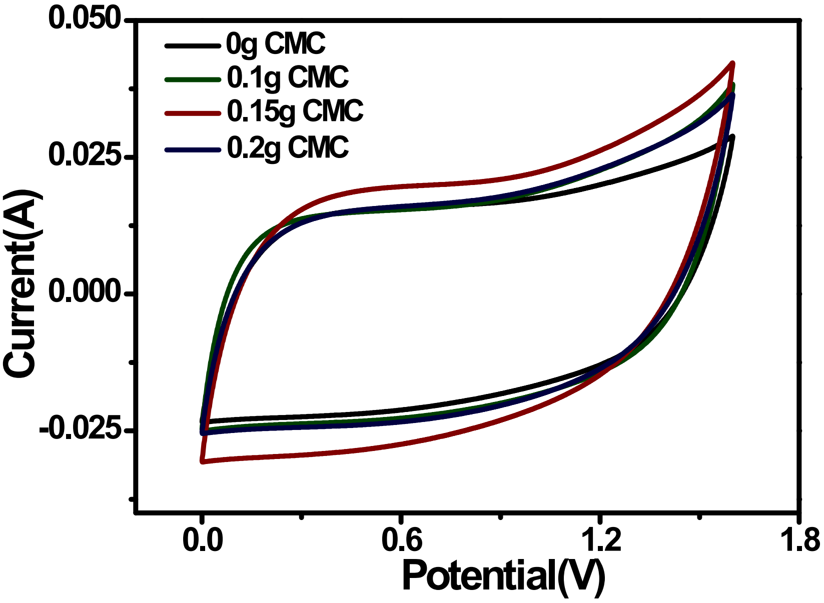

Figure S17. The CV curves of the devices based on PVA-CMC$_x$-LC$_{0.15}$ organo-hydrogel with different CMC contents.

Figure S18. (a) The GCD curves and (b) the rate capability of the SCs device based on PVA-CMC$_x$-LC$_{0.15}$ organo-hydrogel with different CMC contents.

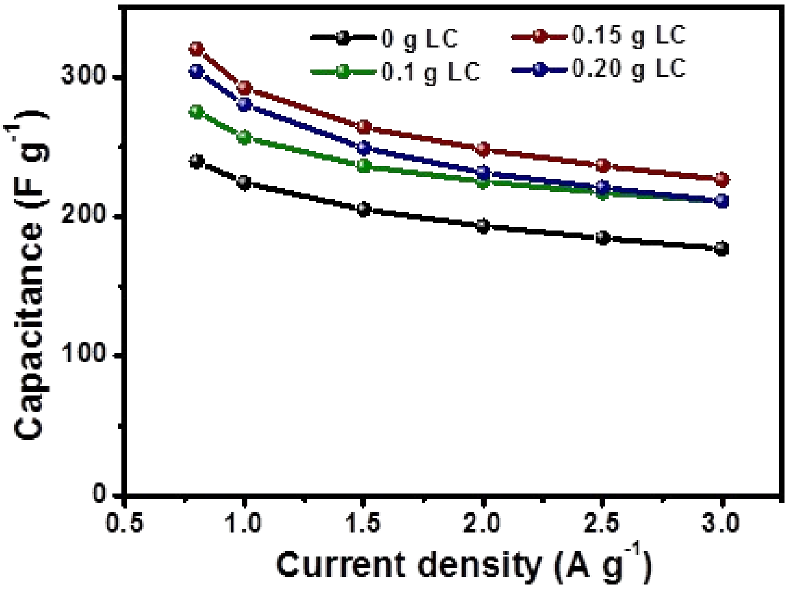

Figure S19. (a) The rate capability of the SCs device based on PVA-CMC$_{0.15}$-LC$_y$ organo-hydrogel with different LC contents.

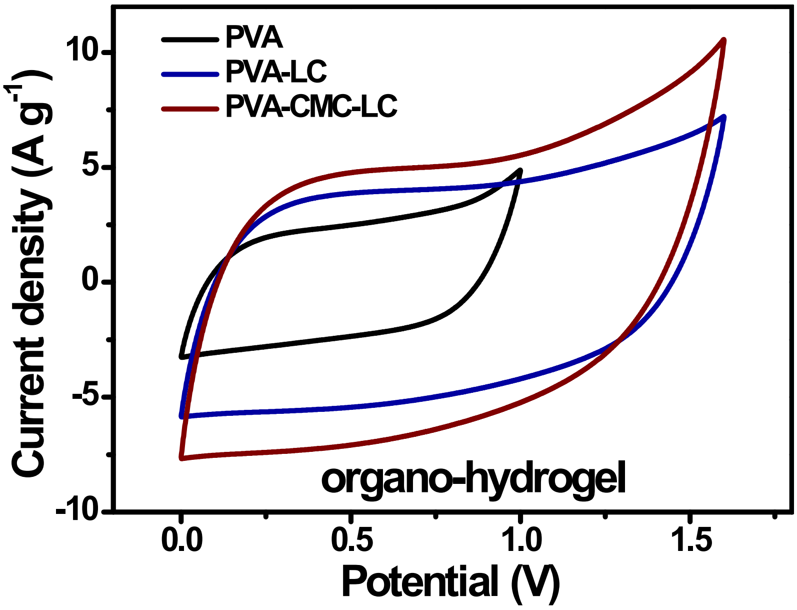

Figure S20. The CV curves of the device based on PVA, PVA-LC and PVA-CMC-LC organo-hydrogel.

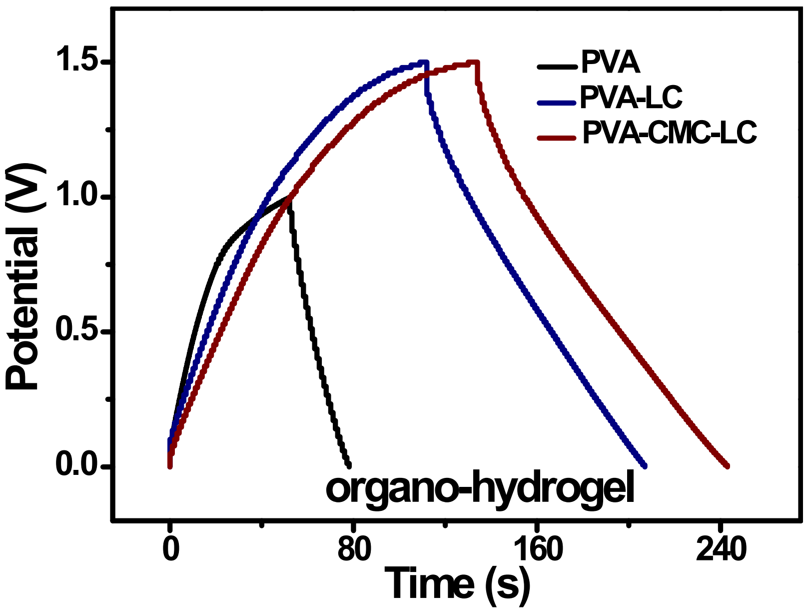

Figure S21. The GCD curves of the device based on PVA, PVA-LC and PVA-CMC-LC organo-hydrogel.

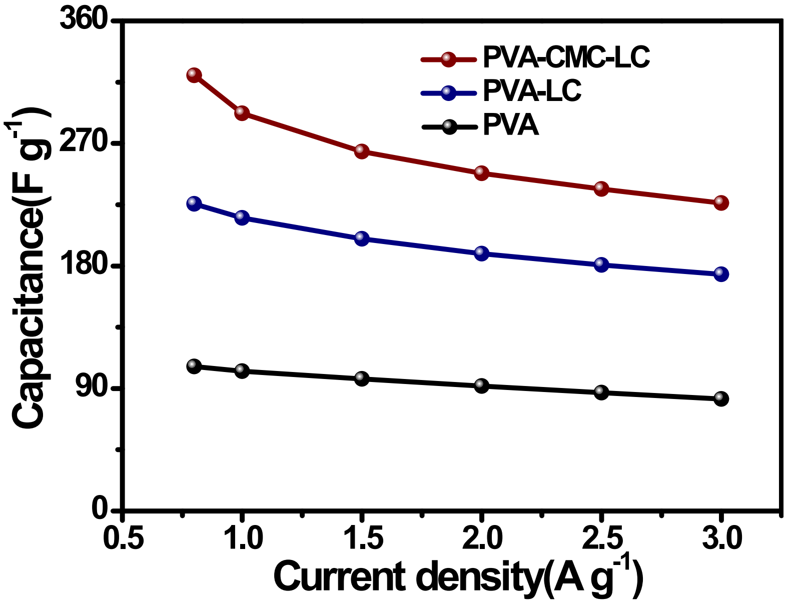

Figure S22. The rate capability of PVA, PVA-LC, PVA-CMC-LC organo-hydrogel SCs devices.

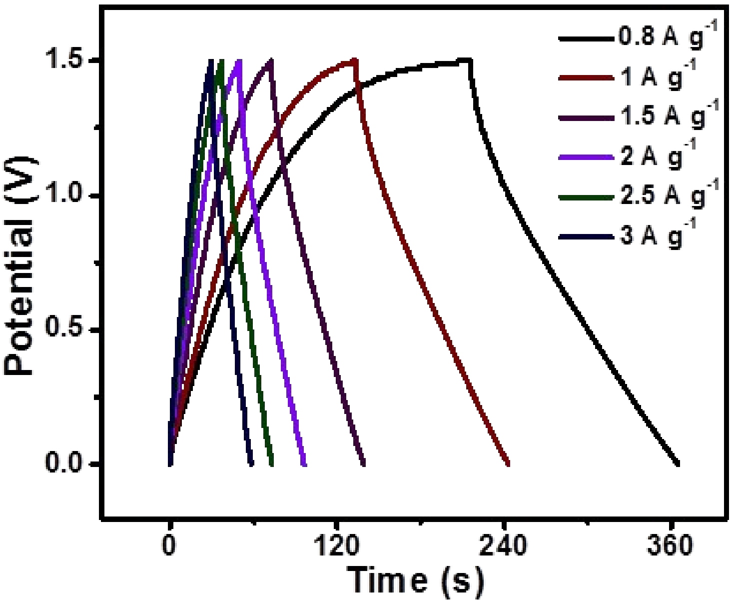

Figure S23. The GCD curves of PVA-CMC-LC organo-hydrogel SCs devices at various current densities.

Table S6. Comparison in cycle stability of the SCs devices based on PVA-CMC-LC organo-hydrogel and other previous reports.

Electrolytes	**Cycle number**	**Retention rate**	**References**
PVA-CMC-LC	10 K	75%	This work
PVA-KOHeK_3[Fe $(CN)_6$]	1 K	89.3%	10
PEDOT: PSS 6.3 wt%	5 K	70%	11
Azo-PAM/α-CDP/LiCl	10 K	68%	12
PVA-AA-S	5 K	80%	13
PVA–H_2SO_4–ARS	1 K	78%	14
PIL/IL-GPE	5 K	70%	15
PPDE-LiCl-EV	2 K	66%	16
PAM/SA	5 K	78%	17

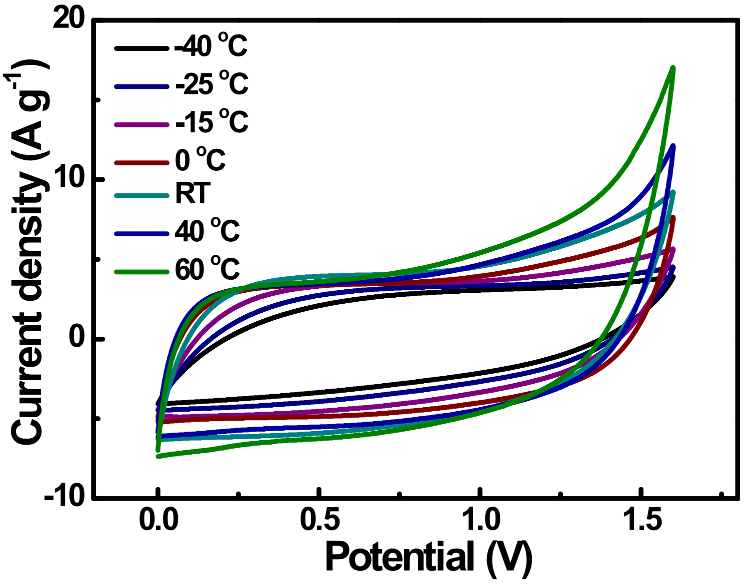

Figure S24. The CV curves of PVA-CMC-LC organo-hydrogel SCs devices at different temperatures from -40 to 60 °C.

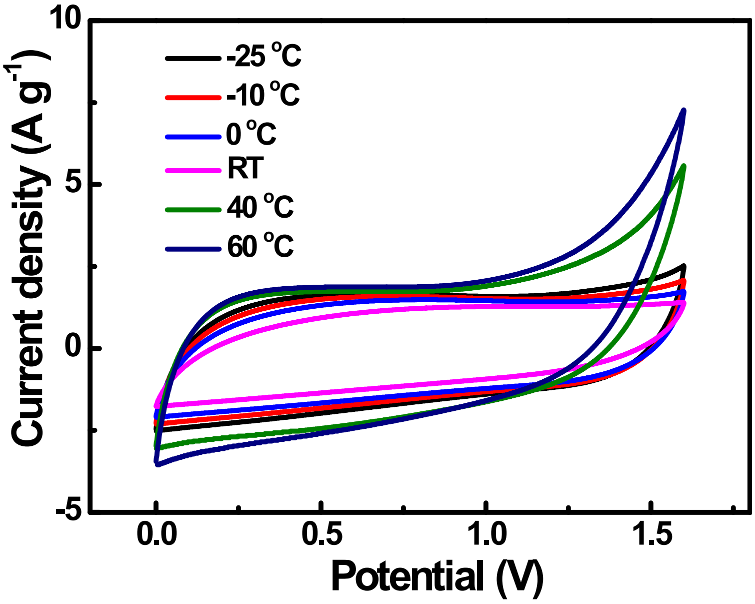

Figure S25. The CV curves of PVA-CMC-LC hydrogel SCs device at a wide temperature range from -25 to 60 °C.

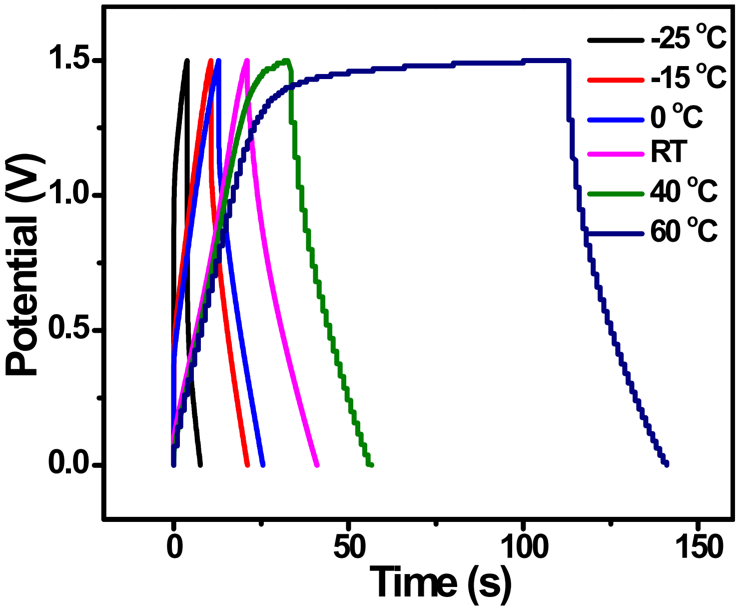

Figure S26. GCD curves of PVA-CMC-LC hydrogel at a wide temperature range from -25 to 60 °C.

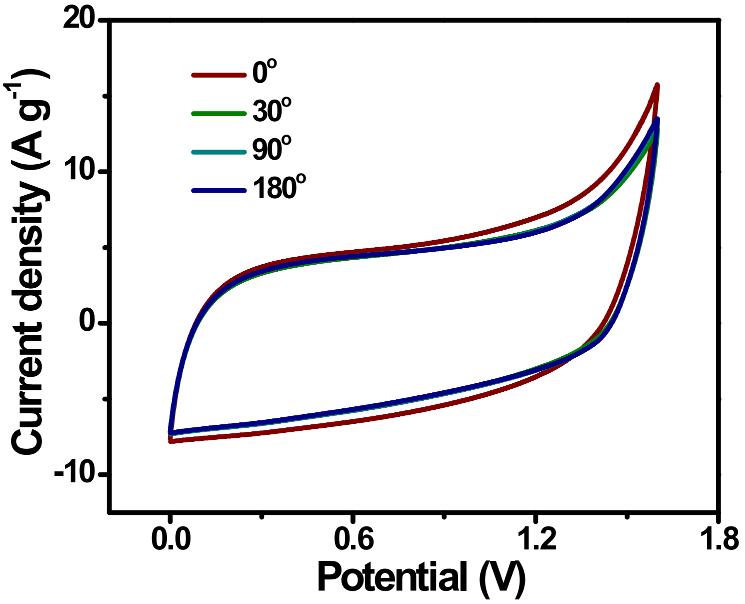

Figure S27. The CV curves of the soft device under different bending angles.

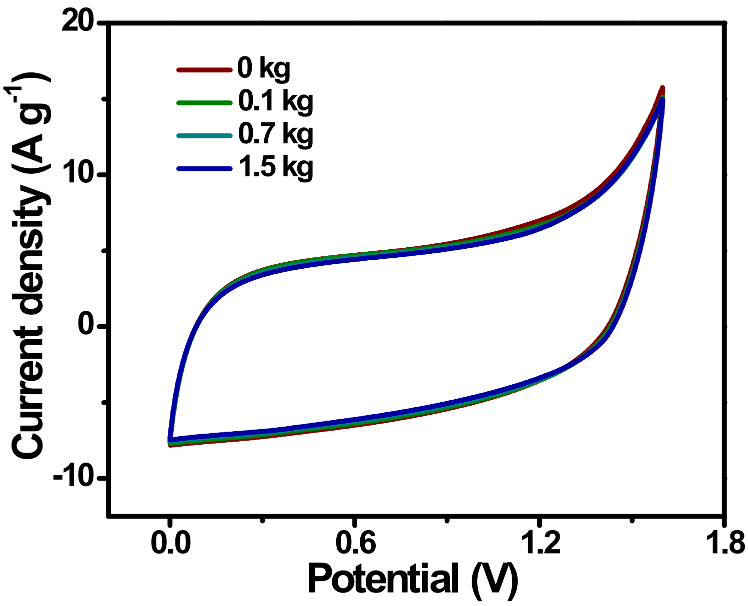

Figure S28. The CV curves of the soft device under different heavy loads.

Reference

1 G. Li, X. Zhang, M. Sang, X. Wang, D. Zuo, J. Xu, H. Zhang, J. Energy Storage, 2021, **33**, 101931.

2 H. Peng, X. Gao, K. Sun, X. Xie, G. Ma, X. Zhou, Z. Lei, Chem. Eng. J., 2021, **422**, 130353.

3 L. Fang, Z. Cai, Z. Ding, T. Chen, J. Zhang, F. Chen, J. Shen, F. Chen, R. Li, X. Zhou, Z. Xie, ACS Appl. Mater. Interfaces, 2019, **11**, 21895-21903.

4 Y. Guo, X. Zhou, Q. Tang, H. Bao, G. Wang, P. Saha, J. Mater. Chem. A, 2016, **11**, 8769-8776.

5 R. Na, Y. Liu, N. Lu, S. Zhang, F. Liu, G. Wang, Chem. Eng. J., 2019, **374**, 738-747.

6 J. Nan, G. Zhang, T. Zhu, Z. Wang, L. Wang, H. Wang, F. Chu, C. Wang, C. Tang, Adv. Sci., 2020, **7**, 2000587.

7 Z. Liu, G. Liang, Y. Zhan, H. Li, Z. Wang, L. Ma, Y. Wang, X. Niu, C. Zhi, Nano Energy, 2019, **58**, 732-742.

8 Z. Shi, Y. Zhang, L. Jia, Q. Zhang, X. Xu, ACS Appl. Mater. Interfaces, 2018, **10**, 36028-36036.

9 X. Li, D. Lou, H. Wang, X. Sun, J. Li, Y. N. Liu, Adv. Funct. Mater., 2020, **30**,

2007291.

10 G. Ma, J. Li, K. Sun, H. Peng, J. Mu, Z. Lei, J. Power Sources, 2014, **256**, 281-287.

11 C.-C. Shih, Y.-C. Lin, M. Gao, M. Wu, J. Power Sources, 2019, **426**, 205-215.

12 J. Kim, J. W. Kim, S. Kim, K. Keum, J. Park, Y. R. Jeong, S. W. Jin, J. S. Ha, Chem. Eng. J., 2021, 422, 130121.

13 H. Yu, N. Rouelle, A. Qiu, J. A. Oh, D. M. Kempaiah, J. D. Whittle, M. Aakyiir, W. Xing, Ma, J. Ma, ACS Appl. Mater. Interfaces, 2021, **12**, 37977-37985.

14 K. Sun, F. Ran, G. Zhao, Y. Zhu, Y. Zheng, Ma, M. Ma, X. Zheng, G. Ma, Z. Lei, RSC Adv., 2016, **6**, 55225–55232.

15 S. A. Alexandre, G. G. Silva, R. Santamaría, J. P. C. Trigueiro, R. L. Lavall, Electrochim. Acta, 2019, **299**, 789-799.

16 S.-E. Hyeon, J. Y. Seo, J. W. Bae, W.-J. Kim, C.-H. Chung, Electrochim. Acta, 2019, **319**, 672- 681.

17 Q. Fu, S. Hao, L. Meng, F. Xu, J. Yang, ACS Nano, 2021, **15**, 18469−18482.

18 X. Zhu, C. Ji, Q. Meng, H. Mi, Q. Yang, Z. Li, N. Yang, J. Qiu, Small, 2022, 2200055.

19 H. Cui, H. Mi, C. Ji, F. Guo, Y. Chen, D. Wu, J. Qiu, H. Xie, J. Mater. Chem. A., 2021, **9**, 23941–23954.

20 J. Zeng, L. Dong, W. Sha, L. Wei, X. Guo, Chem. Eng. J., 2020, **383**, 123098.

21 J. Wang, X. Li, J. Yang, W. Sun, Q. Ban, L. Gai, Y. Gong, Z. Xu, L. Liu, ChemSusChem, 2021, **14**, 2056–2066.

22 S. Wu, D. Lou, H. Wang, D. Jiang, X. Fang, J. Meng, X. Sun, J. Li, Chem. Eng. J., 2022, **435**, 135057.

23 Q. Hua, Xiuting. Shia, K. Sunb, S. Cuia, H.- A. Hamoudaa, W, Zhanga, H. Penga, G. Maa, J. Alloys Compd., 2022, **909**, 164646.

24 S. Wang, D. Zhang, X. He, J. Yuan, W. Que, Y. Yang, I. Protsak, X, Huang, C. Zhang, T. Lu, P. Pal, S. Liu, S.-Y. Zheng, J. Yang, Chem. Eng. J., 2022, **438**, 135607.